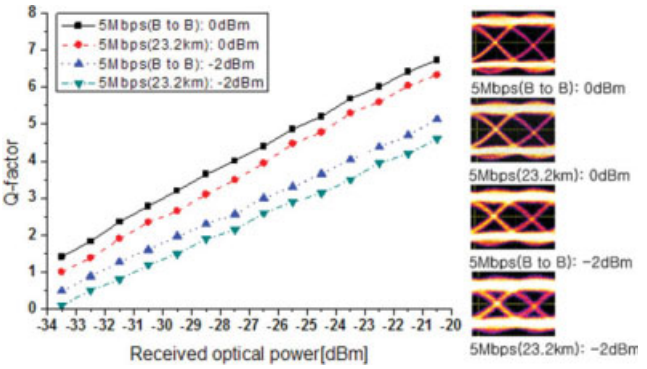

Figure 8 Measured *Q*-factor performance for uplink baseband data signal of 5 Mbps. [Color figure can be viewed in the online issue, which is available at www.interscience.wiley.com]

compared to the downlink signal because the modulation efficiency is better than the detection efficiency of the EAM.

5. CONCLUSIONS

A novel scheme that VLC link is connected with 23.2-km optical link by an EAT is proposed. The feasibility of applying the VLC link to the existing optical access network is verified for the first time. By using a dual function of the EAT, 5 Mbps downlink and uplink data transmission of wireless VLC link based on an optical access network is demonstrated experimentally. The error-free wireless transmission of the VLC link was achieved after 23.2-km transmission for 5 Mbps downlink baseband data and uplink baseband data. However, *Q*-factor performance is degraded under the condition with an ambient light. There are some challenges to overcome, but this proposed system can be useful for applying the VLC link to the optical wireless communication. Further, the optimization of the transmitter and the receiver for VLC link is required, and these are expected to yield further improvements in distance, coverage area, and error performance.

ACKNOWLEDGMENT

This work was supported by Seoul R&BD Program of Korea (No. NT080505).

REFERENCES

1. C.P. Kno, R.M. Fletcher, T.D. Owentowski, M.C. Lardizabal, and M.G. Craford, High performance ALGaInP visible light-emitting diodes, Appl Phys Lett 57 (1990), 2937–2939.
2. T. Komine and M. Nakagawa, Integrated system of white LED visible-light communication and power-line communication, IEEE Trans Consum Electron 49 (2003), 71–79.
3. P. Amirshahi and M. Kavehrad, Broadband access over medium and low voltage power-lines and use of white light emitting diodes for indoor communications, Proc IEEE CCNC, 2006, pp. 897–901.
4. T. Komine and M. Nakagawa, Fundamental analysis for visible-light communication system using LED lights, IEEE Trans Consum Electron 50 (2004), 100–107.
5. G. Jee, R.D. Rao, and Y. Cern, Demonstration of the technical viability of PLC systems on medium-and low-voltage lines in the United States, IEEE Communications Magazine, May 2003, pp. 108–112.
6. W. Liu, H. Widmer, and P. Raffin, Broadband PLC access systems and field deployment in European power line networks, IEEE Communications Magazine, May 2003, pp. 114–118.
7. L. Nöel, D. Wake, D.G. Moodie, D.D. Marcenac, L.D. Westbrook, and D. Nesset, Novel techniques for high-capacity 60-GHz fiber-radio transmission systems, IEEE Trans Microwave Theory Tech 45 (1997), 1416–1423.
8. G. Keiser, Optical fiber communications, McGraw-Hill, New York, NY 2000.

FAST AND ACCURATE CALCULATION OF TRANSMISSION COEFFICIENTS FOR AN EBG MICROSTRIP STRUCTURE

Shao Ying Huang and Yee Hui Lee
Communication Research Laboratory, School of Electrical and Electronic Engineering, Nanyang Technological University, Singapore 639798; Corresponding author: huan0104@ntu.edu.sg

Received 17 June 2009

ABSTRACT: *In this article, an approach is proposed to provide an accurate and fast calculation on the transmission coefficients of an electromagnetic band-gap (EBG) structures where patches are periodically inserted into the microstrip line (capacitive loaded EBG microstrip structure). The stopband performance, such as the center frequency, bandwidth, and attenuation, of these EBG structures can be predicted at a high degree of accuracy through the calculation of the transmission coefficient. The dispersion relation of electromagnetic waves in the structure is derived, plotted, and analyzed. The grating nature of the structure is demonstrated. This approach can be applied to periodic microstrip structures of a similar nature to simplify the analysis and design procedures.* © 2010 Wiley Periodicals, Inc. Microwave Opt Technol Lett 52: 793–797, 2010; Published online in Wiley InterScience (www.interscience.wiley.com). DOI 10.1002/mop.25046

Key words: *electromagnetic band-gap structures; EBG; planar passive filters; capacitive loaded EBG microstrip structures; low-pass filters; band-stop filters; microstrip filters*

1. INTRODUCTION

Wireless communications have been developing at an accelerating rate in the past decade. With the advance in technology, wireless systems require high-performance circuits and components that are miniaturized. With the increase in the number of wireless users, the requirement on filters in modern communication systems has become stringent. Besides a small physical size, they are required to have sharp cutoff, high attenuation in the stopband, low insertion loss in the passband, and no spurious.

Planar electromagnetic band-gap (EBG) microstrip structures have played an important role in filter designs since they are introduced in 1998 [1]. An EBG microstrip structure is a microstrip line with periodic cells arranged along the direction of the microstrip line. It exhibits a wide stopband at a center frequency that is determined by the period of the cells. It is convenient to use an EBG filter to suppress unwanted frequencies over a wide frequency range [2].

In an EBG microstrip structure, the periodic cells along the microstrip line are used to modulate the microstrip line, thus locally altering its effective permittivity. The modulation creates alternate passbands and stopbands in the frequency response of the structure. These periodic cells can be in the form of etched patches in the ground plane of a microstrip line with a 1-D [3] or 2-D pattern [1]. They can also be in the form of patches inserted in the microstrip line [4–6], which is known as periodic structure with shunt-capacitive loading [4] or capacitive loaded transmission line [5]. Grating structures have been applied in the field of optics for decades [7]. Lately, they have been applied in

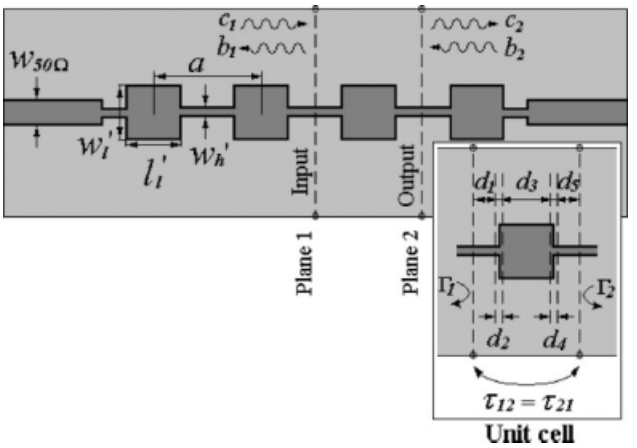

Figure 1 The schematic of a capacitive loaded EBG microstrip structure

millimeter waves technology [8] and coplanar waveguide (CPW) technology [9]. An EBG microstrip structure can be seen as the applications of gratings in microstrip line technology. It satisfies the Bragg reflection condition.

An EBG structure with uniform cells shows high ripple level in the passband due to the periodicity, mismatch at the input, and additional reflections caused by the cells. Fortunately, it has been shown that these ripples can be eliminated effectively by applying tapering techniques [6]. Planar EBG microstrip structures are high-performance band-stop filters [3] or low-pass filters [10] that provide high selectivity and a wide stopband with high attenuation. It is simple to design, small in physical size, and compatible with monolithic circuits. Recently, EBG structures are applied to the design of band-pass filters [5] and ultra-wideband band-pass filter [4] to suppress spurious in the stopband. EBG structures are widely used in filter designs. However, full-wave simulations are required to predict the stopband performance of the structure, such as the bandwidth, center frequency, and attenuation. The simulations are time consuming.

In this article, an approach is proposed to calculate the transmission coefficients of an EBG structure with inserted patches in the microstrip line (capacitive loaded EBG microstrip structure) so as to derive the stopband. The periodic waves of the structure are analyzed and the dispersion relation of the electromagnetic waves is plotted. The dispersion relation is used to show the grating nature of the EBG structure. This proposed model can help to simplify the analysis of EBG microstrip structures. It can easily be generalized and applied to facilitate and accelerate the computer-aided designs of periodic microstrip structures of this type.

2. STOPBAND PREDICTION AND DISPERSION RELATION

An EBG structure is an application of gratings onto a microstrip line. It satisfies the Bragg reflection condition [7, 8]:

$$\lambda = 2a \cdot n \tag{1}$$

where λ is the wavelength of the reflected wave, a is the distance between two successive cells (defined as the period of the structure), and n is the refractive index $n = \sqrt{\varepsilon_r \mu_r}$. Therefore, with a fixed period of the structure, the center frequency of its stopband can be estimated using (1). However, Eq. (1) provides no other information about the stopband, such as the attenuation and the bandwidth.

In this section, we present an approach to predict the stopband performance of a capacitive loaded EBG microstrip structure (Fig. 1), including its center frequency, bandwidth, and attenuation. This is done by obtaining the *ABCD* matrix and the characteristic impedance of the periodic structure. In Section 2.1, an equivalent circuit is proposed to obtain an *ABCD* matrix of a unit cell of the structure, according to its geometry. An overall *ABCD* matrix of the periodic EBG structure can then be obtained by cascading several unit cells. In Section 2.2, periodic waves in the structure are analyzed to obtain the characteristic impedance. With an *ABCD* matrix and the characteristic impedance of the periodic structure, its transmission coefficient at each frequency can be calculated. The dispersion relation of the structure is expressed and plotted.

2.1. The ABCD *Matrix of a Unit Cell*

Figure 1 shows a capacitive loaded EBG microstrip structure with four cells ($m = 4$). An EBG unit cell is taken out with terminal plane 1 and 2 midway between two successive inserted patches. To obtain the *ABCD* matrix for the unit cell shown in Figure 1, the unit cell is further divided into five sections of length d_i (i = 1–5) that are cascaded; the first section is a narrow microstrip line section with a length of $d_1 = (a - l_l')/2$; the second section takes into account the narrow to wide discontinuity where $d_2 \approx 0$; the third section is a wide microstrip line section with $d_3 = l_l'$ the forth section is another discontinuity from wide to narrow with $d_4 \approx 0$; and the last section is a narrow microstrip line section with $d_5 = d_1 = (a - l_l')/2$.

The *ABCD* matrix of a microstrip line section (in this contest, the first, the third, or the fifth sections) can be expressed as [11],

$$\begin{bmatrix} A & B \\ C & D \end{bmatrix}_{\text{mi}} = \begin{bmatrix} \cos\beta l & jZ_0 \sin\beta l \\ jY_0 \sin\beta l & \cos\beta l \end{bmatrix} \tag{2}$$

where the subscript, mi denotes the ith microstrip line section. The *ABCD* matrix of the two microstrip step discontinuity (narrow to wide and wide to narrow) is obtained as followed. Figures 2(a) and 2(b) shows the step-up discontinuity (narrow to wide) and the step-down discontinuity (wide to narrow), respectively. In Figures 2(a) and 2(b), W_{i-1} and W_i are the widths of the microstrip line sections from left to right. The subscripts, $(i + 1)$ and i are the indices for the microstrip line sections. Each of them can be modeled using the T-network as shown in Figure 2(c) [12]. As can be seen in Figure 2(c), L_{i-1} and L_i

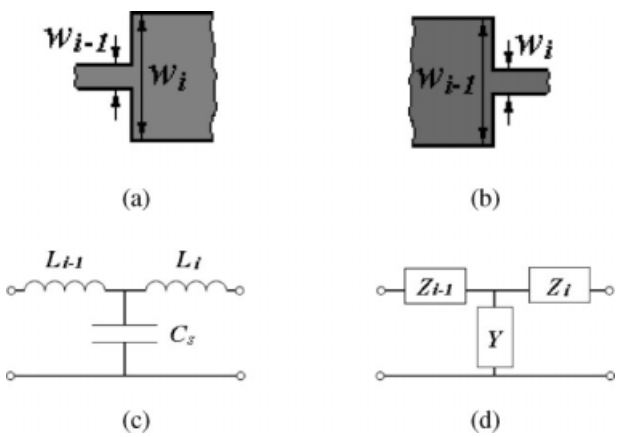

Figure 2 (a, b) Microstrip step discontinuities and (c, d) its equivalent circuits

correspond to the inductance of the microstrip line section with a width of W_{i-1} and of W_i of the step discontinuity as shown in Figures 2(a) and 2(b), respectively. The excess capacitance due to the step discontinuity is C_s. The inductances, L_{i-1} and $L_{i,}$ can be estimated using the Eqs. (3)–(6) below.

$$L_s = 0.000987h\left(1 - \frac{Z_{0W}}{Z_{0N}}\sqrt{\frac{\epsilon_{reW}}{\epsilon_{reN}}}\right)^2 (\text{nH}) \tag{3}$$

$$L_{i-1} = \frac{L_{W_{i-1}}}{L_{W_{i-1}} + L_{W_i}} L_s \tag{4}$$

$$L_i = \frac{L_{W_i}}{L_{W_{i-1}} + L_{W_i}} L_s \tag{5}$$

$$L_{W_i} = \frac{Z_{0mi}\sqrt{\epsilon_{rei}}}{c} (\text{H/m}) \tag{6}$$

where Z_{0W} and ϵ_{reW} are the characteristic impedance and the effective dielectric constant of the wide microstrip line section, whereas Z_{0N} and ϵ_{reN} are those of the narrow microstrip line section. The thickness of the substrate, h is in micrometer. Z_{0m} and ϵ_{re} are the characteristic impedance and the effective dielectric constant of the microstrip line. In (6), L_{W_i} is the inductance per unit length of the microstrip line of width W_i and c is the speed of light in free space. The excess capacitance C_s can be estimated by using (7) below,

$$C_s = 0.00137\frac{\sqrt{\epsilon_{reW}}}{Z_{0W}}\left(1 - \frac{W_N}{W_W}\right)h\left[\frac{\epsilon_{reW} + 0.3}{\epsilon_{reW} - 0.258}\right] \times \left[\frac{W_W/h + 0.264}{W_W/h + 0.8}\right](\text{pF}) \tag{7}$$

where h is in micrometer, W_N and W_W are the widths of the narrow and the wide microstrip line sections, respectively.

The T-network in Figure 2(c) is presented in an alternative way using reactance Z_{i-1} and Z_i and a susceptance Y and is shown in Figure 2(d). Therefore, the *ABCD* matrix of this network for the step discontinuity can be obtained as shown below,

$$\begin{bmatrix} A & B \\ C & D \end{bmatrix}_{si} = \begin{bmatrix} 1 & Z_{i-1} \\ 0 & 1 \end{bmatrix}\begin{bmatrix} 1 & 0 \\ Y & 1 \end{bmatrix}\begin{bmatrix} 1 & Z_i \\ 0 & 1 \end{bmatrix} = \begin{bmatrix} 1 + Z_{i-1}Y & Z_i + Z_iZ_{i-1}Y + Z_{i-1} \\ Y & Z_iY + 1 \end{bmatrix} \tag{8}$$

where the subscript, *si* denotes the *i*th step discontinuity. As the five sections are cascaded to form a unit cell, the *ABCD* matrix for the unit cell can be obtained by multiplying the *ABCD* matrix of each section as follows,

$$\begin{bmatrix} A & B \\ C & D \end{bmatrix}_c = \begin{bmatrix} A & B \\ C & D \end{bmatrix}_{m1} \cdot \begin{bmatrix} A & B \\ C & D \end{bmatrix}_{s1} \cdot \begin{bmatrix} A & B \\ C & D \end{bmatrix}_{m2} \cdot \begin{bmatrix} A & B \\ C & D \end{bmatrix}_{s2} \cdot \begin{bmatrix} A & B \\ C & D \end{bmatrix}_{m3} \tag{9}$$

where the subscript c denotes cell. $\begin{bmatrix} A & B \\ C & D \end{bmatrix}_{m1}$, $\begin{bmatrix} A & B \\ C & D \end{bmatrix}_{m2}$, and $\begin{bmatrix} A & B \\ C & D \end{bmatrix}_{m3}$ can be obtained by using (2) whereas $\begin{bmatrix} A & B \\ C & D \end{bmatrix}_{s1}$ and $\begin{bmatrix} A & B \\ C & D \end{bmatrix}_{s2}$ can be obtained by using (10). Therefore, the overall *ABCD* matrix of the EBG shown in Figure 1 can be obtained by cascading those of the four unit cells by using (11). Based on the *ABCD* matrix, two-port network parameters, such as the [*Z*] matrix and the [*Y*] matrix of the structure can be obtained readily. For the prediction of the stop-band performance, or in other words, for obtaining the *S*-parameters at each frequency, the characteristic impedance of the periodic structure, Z_c, is required. In the following section, Z_c is obtained for the capacitive loaded EBG microstrip structure by analyzing the periodic waves in the structure. The *S*-parameters are calculated and plotted. The dispersion relation of the structure is obtained and plotted. It is used to show the grating nature of the EBG microstrip structure.

2.2. Characteristic Impedance and Dispersion Relation of an EBG Microstrip Structure

The characteristic impedance of the EBG structure in Figure 1 can be obtained by analyzing periodic waves in the structure [13]. The unit cell shown in Figure 1 has a reflection coefficient Γ_1 and Γ_2 at the two terminal planes 1 (input) and 2 (output), respectively. c_1 and b_1 are the amplitude of the forward- and the backward-propagating wave at the input, respectively, whereas c_2 and b_2 are the amplitudes of the waves at the output. The transmission coefficients between the two terminal planes are τ_{12} and τ_{21}. Due to the reciprocity of the unit cell, $\tau_{12} = \tau_{21}$. The wave amplitudes are related using a wave matrix [13]. For a capacitive loaded EBG microstrip line structure, it consists of cascaded periodic unit cells. With a wave propagating down the structure, c_1 and c_2, b_1 and b_2 are related by (10) and (11), respectively, as shown below,

$$c_2 = e^{-\gamma_c a}c_1 \tag{10}$$

$$b_2 = e^{-\gamma_c a}b_1 \tag{11}$$

where $\gamma_c = \alpha_c + j\beta_c$ is the propagation constant.

Besides the wave matrix, the amplitudes, c_1, c_2, b_1, and b_2 can also be related through voltages and currents of the network. Figure 3 shows the equivalent T-network for the unit cell with input and output voltages and currents. The relation between c_1 and b_1 and that between c_2 and b_2 are expressed as follows,

$$V_1 = c_1 + b_1 \tag{12}$$

$$V_2 = c_2 + b_2 \tag{13}$$

$$I_1 = (c_1 - b_1)Y_w \tag{14}$$

$$I_2 = (c_2 - b_2)Y_w \tag{15}$$

where Y_w is the wave admittance. Based on (12)–(15), wave matrix can be translated into impedance matrix [*Z*]. With algebraic manipulations, the characteristic impedance of the structure can be expressed as shown in (16) below [13],

$$Z_c = \frac{Z_{11} - Z_{22}}{2} + Z_{12}\sin h\gamma_c a \tag{16}$$

where $\sin h\gamma_c a = (\cos h^2\gamma_c a - 1)^{1/2}$. The relation between γ_c and [*Z*] can be expressed using (17) [13].

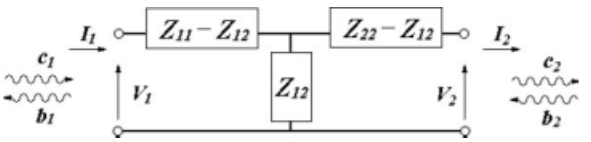

Figure 3 The equivalent T-network for the unit cell of a capacitive loaded EBG microstrip structure in Figure 1

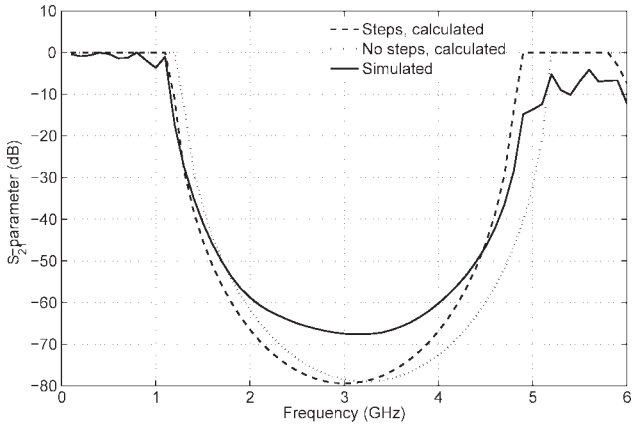

Figure 4 The simulated and calculated S_{21}-parameters of the capacitive loaded EBG microstrip structure ($f_c = 3.1$ GHz)

$$\cos h\gamma_c a = \frac{Z_{11} + Z_{22}}{2Z_{12}} \tag{17}$$

Based on (16) and (9), the impedance of the EBG microstrip structure is related to the geometry of the structure and can be obtained. Therefore, the *S*-parameters of the EBG structure can be calculated based on the dimensions of the structure. Equation (17) expresses the dispersion relation of the EBG structure.

2.3. Prediction on S-*Parameters*

A four-cell capacitive loaded EBG microstrip structure as shown in Figure 1 with a center frequency of the stopband at 3 GHz is designed. Taconic ($\epsilon_r = 2.46$, $h = 30.5$ mils) is used as the substrate. The width of the microstrip line at the input and the output port is set to correspond to a characteristic impedance of 50 Ω at 3 GHz. The period of the structure a is determined by applying (1). Both l_l' and w_l' are set to $0.5a$ corresponding to an optimal filling factor of 0.5 [1]. The width of the microstrip line section between two successive inserted patches w_h' is set to 0.6 mm. The EBG microstrip structure is simulated using the method of moment base software, advanced design system (ADS) [14]. The solid line in Figure 4 shows its simulated S_{21}-parameters. The center frequency and the 15 dB bandwidth of the stopband are found to be 3.1 and 3.7 GHz, respectively. The attenuation at the center of the stopband is 67.6 dB. The lower and the upper 15 dB-cutoff frequencies of this EBG structure are found to be 1.2 and 4.9 GHz, respectively.

To calculate the dispersion relation of this EBG structure, Z_{0m} and ϵ_{re} of the narrow and wide microstrip line sections are estimated using Linecalc in ADS at different frequencies based on their physical dimension [14]. The propagation constant of the microstrip lines, β_n and β_w, are determined accordingly. By applying (2)–(9), the *ABCD* matrix for the unit cell of the capacitive loaded EBG microstrip structure is obtained. *S*-parameters are calculated based on the *ABCD* matrix and (16) for the characteristic impedance, Z_c. Figure 4 shows the calculated S_{21}-parameters. The calculated S_{21}-parameters without taking into consideration of the step discontinuities in (9) are included for a comparison. The center frequencies and 15 dB-cutoff frequencies of the three curves in Figure 4 are compared to evaluate the accuracy of the calculation. As can be seen in Figure 4, for the curve that takes into account the step discontinuities, its lower and the upper 15 dB-cutoff frequencies are at 1.2 and 4.8 GHz, respectively. The center frequency of the stopband is at 3.1 GHz. These calculated results are in a good agreement with the simulated results (15 dB-cutoff frequencies at 1.2 and 4.9 GHz, the center frequency at 3.1 GHz). For the curve without taking into account the step discontinuities, its 15 dB-cutoff frequencies are at 1.3 (lower) and 5.1 GHz (upper). It has the stopband centered at 3.2 GHz. Compared to the simulation results, it shows a shift in center frequency of the stopband and a larger bandwidth. The comparison shows the importance of the step discontinuity for the calculation of the stopband performance.

The results reveal that the proposed approach for deriving the stopband performance of a capacitive loaded EBG microstrip structure is of high accuracy. It provides information on the center frequency, the bandwidth, and the attenuation of the stopband. The accuracy of the prediction is increased by taking into account the effect of the step discontinuities in the structure. This approach can be further extended to other periodic microstrip structure by modifying the circuit model in Section 2.1.

2.4. Plot of Dispersion Relation

The dispersion relation for the capacitive loaded EBG microstrip structure is calculated using (18) and plotted in Figure 5. As can be seen in Figure 5, the EBG structure shows maximum β_c at both edges of the stopband, which is similar to a typical dispersion relation of a periodically loaded transmission line [15]. The parameters of the structure will be analyzed in detail to examine its grating nature.

Due to the lossless network that is assumed in every section of the unit cell, *Z*-parameters are all purely imaginary. Thus, $\cos h\gamma_c a$ in (18) is a real number. As $\cos h\gamma_c a = \cos h[(\alpha_c + j\beta_c)a] = \cos h\alpha_c a \cos\beta_c a + j\sin h\alpha_c a \sin\beta_c a$, there are two possible cases:

- Case 1: $\alpha_c \neq 0$, $\beta_c = 0$ ($\cos h\gamma_c a > 0$) or $\beta_c a = \pi$ ($\cos h\gamma_c a < 0$). The wave is evanescent. In the short distance it propagates, there is no change in phase when $\beta = 0$ and there is a change in phase when $\beta = \pi$. It defines the stopbands of the structure.
- Case 2: $\alpha_c = 0$, $\beta_c \neq 0$. The wave is propagating without attenuation. It defines the passbands of the structure.

Figure 5 shows a plot of the calculated $\beta_c a$ versus $k_0 a$. As can be seen in Figure 5, there is a prominent stopband at a center frequency of 3.1 GHz.

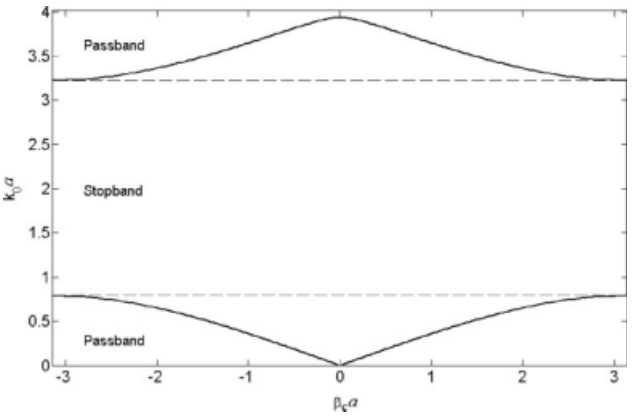

Figure 5 Dispersion relation of the capacitive loaded EBG microstrip structure in Figure 1

TABLE 1 Summaries on Characteristics of a Capacitive Loaded EBG Microstrip Structure

	α_c	β_c	A	B	Z_c
Passband	$= 0$	$\neq 0$	$\|A\| < 1$	Purely imaginary	Real
Stopband	$\neq 0$	$\beta_c = 0/\beta_c a = \pi$	$\|A\| > 1$	Purely imaginary	Purely imaginary

Table 1 summarizes the passband and stopband characteristics of the capacitive loaded EBG microstrip structure based on calculated results. A and B are the parameters in the $ABCD$ matrix. They are related to γ_c, β_c, and Z_c by the expressions,

$$A = \frac{e^{\alpha_c l} + e^{-\alpha_c l}}{2}\cos(\beta_c l) + j\frac{e^{\alpha_c l} - E^{-\alpha_c l}}{2}\sin(\beta_c l) \quad (18)$$

$$B = jZ_c\left[\frac{e^{\alpha_c l} + e^{-\alpha_c l}}{2}\sin(\beta_c l) - j\frac{e^{\alpha_c l} - e^{-\alpha_c l}}{2}\cos(\beta_c l)\right] \quad (19)$$

where l is the length of the transmission line. Z_c in (16) is related to A-parameter as below for a reciprocal network ($Z_{11} = Z_{22}$),

$$Z_c = Z_{12}(A^2 - 1)^{\frac{1}{2}} \quad (20)$$

Equation (20) is obtained based on $Z_{11} = A/C$, $Z_{12} = (AD - BC)/C$, and $AD - BC = 1$.

As shown in Table 1, besides the differences in α_c and β_c between the passband and the stopband, it is observed that A-parameters are in different range of value for different frequency range, B-parameters are purely imaginary at all frequencies, and $Z_c s$ are real in the passband and purely imaginary in the stopband. Based on (18)–(20), it is the difference in γ_c and β_c that leads to the different range of value for A-parameters. The different A-parameters result in the real Z_c in the passband and the purely imaginary Z_c in the stopband. The characteristics of γ_c, β_c, and Z_c result in the purely imaginary B-parameters in both the passband and the stopband.

In the capacitive loaded EBG microstrip structure under study, the characteristics of the parameters in the passband and the stopband, such as the propagation constant, characteristic impedance, A- and B-parameters, are the same as the periodic CPWs with inductive loading as reported in [9]. The dispersion relation and the analysis in this section show the grating nature of the EBG structure. The propagation constants of the EBG microstrip structure in the passband and those of the periodically loaded CPW [9] have different trends versus frequency. The EBG microstrip structure has the maxima of β_c at both edges of the stopband, whereas the CPW structure has the maximum value only at the lower edge of the stopband (Figs. 3(a) and 4(a) in [9]).

3. CONCLUSIONS

This article present an approach that provides an accurate and time-saving calculation of the transmission coefficients of a capacitive loaded EBG microstrip structure. It has been shown that the model of the step discontinuity in the structure plays an important role in the calculation. The stopband of the structure can be predicted with a high accuracy. Furthermore, the dispersion relation of electromagnetic waves in the structure is derived, plotted, and analyzed. The grating nature of the structure is shown. With proper modifications of the circuit model, this approach can be extended to other periodic microstrip structures. The proposed approach will simplify the analysis and design procedures of EBG microstrip structures.

REFERENCES

1. V. Radisic, Y. Qian, R. Coccioli, and T. Itoh, Novel 2-D photonic bandgap structure for microstrip lines, IEEE Microwave Guid Wave Lett 8 (1998), 69–71.
2. V. Radisic, Y. Qian, and T. Itoh, Broad-band power amplifier using dielectric photonic bandgap structure, IEEE Microwave Guid Wave Lett 8 (1998), 13–14.
3. F. Falcone, T. Lopetegi, and M. Sorolla, 1-D and 2-D photonic bandgap microstrip structures, Microwave Opt Technol Lett 22 (1999), 411–412.
4. S.W. Wong and L. Zhu, EBG-embedded multiple-mode resonator for UWB bandpass filter with improved upper-stopband performance, IEEE Microwave Wireless Compon Lett 17 (2007), 421–423.
5. J. Garcia-Garcia, J. Bonache, and F. Martin, Application of electromagnetic bandgaps to the design of ultra-wide bandpass filters with good out-of-band performance, IEEE Trans Microwave Theory Tech 54 (2006), 4136–4140.
6. S.Y. Huang and Y.H. Lee, Tapered dual-plane compact electromagnetic band-gap microstrip filter structure, IEEE Trans Microwave Theory Tech 53 (2005), 2656–2664.
7. K. Ogawa, W.S.C. Chang, B. Sopori, and F.J. Rosenbaum, A theoretical analysis of etched grating couplers for integrated optics, IEEE J Quantum Electron QE-9 (1973), 29–42.
8. T. Itoh, Application of gratings in a dielectric waveguide for leacky-wave antennas and band-reject filters, IEEE Trans Microwave Theory Tech MTT-25 (1977), 1134–1138.
9. L. Zhu, Guided-wave characteristics of periodic coplanar waveguides with inductive loading-unit-length transmission parameters, IEEE Trans Microwave Theory Tech 51 (2003), 2133–2138.
10. S.Y. Huang and Y.H. Lee, High performance, compact meander dual planar EBG microstrip lowpass filter design, In Proceedings of the 2nd IASTED International Conference on Antennas, Radar, and Wave Propagation, Banff, Canada, 2005, pp. 77–82.
11. D.M. Pozar, Microwave engineering, international ed., Wiley, New York, 1998.
12. K.C. Gupta, R. Garg, I. Bahl, and P. Bhartia, Microstrip lines and slotlines, 2nd ed., Artech House Inc., Norwood, MA, 1996, pp. 204–208.
13. R.E. Collin, Field theory of guided waves, 2nd ed., IEEE press, New York, 1992.
14. Advanced Design System 2006 A. Agilent Technologies, Available at: www.home.agilent.com 2006.
15. J.A. Kong, Electromagnetic wave theory. EMW Publishing, 2008.

LOW-VOLTAGE/LOW-POWER 7-GHz TRANSFORMER-COUPLED CURRENT-REUSED CMOS QVCO WITH WIDE TUNING RANGE

Yan-Ru Tseng, Tzuen-Hsi Huang, and Shang-Hsun Wu
Department of Electrical Engineering, National Cheng Kung University, 1 University Road, Tainan 70101, Taiwan, Republic of China; Corresponding author: thhuang@ee.ncku.edu.tw

Received 23 June 2009

ABSTRACT: *In this article, we report the design of a transformer-coupled current-reused quadrature voltage-controlled oscillator (QVCO) having low-voltage operation, low-power consumption, and a wide tuning range. An improved trifilar transformer that is fabricated by*